Efficient experimental characterisation of the permeability of fibrous textiles

Elinor Swery, Tom Allen, Sébastien Comas-Cardona, Quentin Govignon, Chris Hickey, Jamie Timms, Loïc Tournier, Andrew Walbran, Piaras Kelly, Simon Bickerton

Efficient experimental characterisation of the permeability of fibrous textiles

Elinor E Swery[1], Tom Allen[1], Sebastien Comas-Cardona[2], Quentin Govignon[1], Chris Hickey[1], Jamie Timms[1], Loic Tournier[3], Andrew Walbran[1], Piaras Kelly[4] and Simon Bickerton[1]

Abstract

Two experimental set-ups used to characterise the in-plane and through-thickness permeabilities of reinforcing textiles have been developed and are presented. Both the experimental testing and data processing techniques used have been selected to ensure that the characterisation is completed in an efficient and robust method, increasing the repeatability of tests while minimising user induced errors as well as the time and resources needed. A number of key results and outputs obtained are presented from tests carried out on a plain woven reinforcing textile with a range of number of layers and at different fibre volume fractions.

Keywords

Permeability, fabrics/textiles, resin transfer moulding

Introduction

Fibre reinforced polymer composite (FRPC) materials are used in a large number of industrial applications. FRPCs consist of two or more distinct materials (generally fibre reinforcement and polymer matrix), forming a material with more desirable properties. For applications where parts are mass produced and high levels of accuracy and repeatability are required, liquid composite moulding (LCM) processes are the preferred manufacturing method.[1] In LCM processes, resin is injected into a mould containing the dry fibrous reinforcement and is left to cure before the final part can be removed from the mould.

The use of LCM simulations as process design tools is increasing in industry. These simulations are used to accurately predict fill time, flow front advancement and dry spot formation, ultimately enabling the production of complex high quality parts using the most efficient parameters.[2] In these simulations, the resin flow during the LCM manufacturing process is commonly modelled using Darcy's law.[3] The relationship between velocity, pressure and permeability is given in equation (1), where $\mathbf{q}$ is the volume averaged Darcy velocity; μ is the fluid viscosity; P is the fluid pressure and $\mathbf{K}$ is the permeability tensor.

$$\mathbf{q} = -\frac{1}{\mu}\mathbf{K}\nabla \mathrm{P} \tag{1}$$

Permeability, $\mathbf{K}$, is a measure of the ability of a reinforcement material to transmit fluids. It is an important material characteristic that determines the flow propagation of the resin during LCM manufacturing processes and is an indispensable input into LCM process simulations.[4] Permeability behaviour of reinforcing textiles is a strong function of the textile's complex architecture.[5] This complexity makes the development of adequate analytical models extremely difficult, therefore many researchers are relying on measurements obtained from experiments.[6]

Many different experimental techniques are presented in literature for the purposes of measuring the permeability behaviour of reinforcing materials.[7–24]

[1]Centre for Advanced Composite Materials, Department of Mechanical Engineering, University of Auckland, New Zealand
[2]Research Institute in Civil Engineering and Mechanics (GeM), UMR CNRS 6183, France
[3]Department of Polymers and Composites Technology & Mechanical Engineering, France
[4]Department of Engineering Science, University of Auckland, New Zealand

Corresponding author:
Simon Bickerton, Centre for Advanced Composite Materials, Department of Mechanical Engineering, University of Auckland, Private Bag 92019, Auckland, New Zealand.
Email: s.bickerton@auckland.ac.nz

These experimental methods can be classified based on the following:

- Measurement direction: in-plane or through-thickness
- Type of flow: radial or rectilinear
- Injection type: constant flow rate or constant pressure
- Fluid utilised: liquid or gas
- Measurement method: discreet or continuous (for different fibre volume fraction (V_f) levels)
- Measurement state: transient (unsaturated) or steady-state (saturated)

In general, permeability experiments are carried out by generating fluid flow through the reinforcing material of interest and measuring the resulting pressure drop and flow rate. These are used with analytical solutions for the specific flow situation that have been derived from Darcy's law,[3] to compute the permeability.

Experimental set-ups that use a constant flow rate injection[25–31] require the monitoring of the resulting pressure gradient. For cases where the experiments are carried out using constant injection pressure[7,13,32–36] the flow front velocity is measured. This is done by either detecting the location of the flow front at regular intervals or through the use of flow meters.

When conducting permeability experiments, it is important to ensure that a slow flow is achieved, typically with a Reynolds number that is significantly less than 1.[37] This is so as to not deviate from the initial assumptions made with regards to Darcy's law.[3]

In order to fully characterise the permeability of a textile, the influence of varying preform structures, compaction levels, shear angles, etc. must be resolved, resulting in a significant test matrix. This results in a time and labour intensive task. It is therefore crucial to ensure that the experimental measurement systems used for the permeability characterisation is efficient and simple to use, as well as providing the most robust results whereby user induced errors are minimised.[37,38]

This article presents two permeability measurement systems that have been developed over a number of years at the Centre for Advanced Composite Materials. These are used to experimentally characterise the in-plane and through-thickness permeabilities of fibre reinforced textiles in an efficient and robust method. During the development of the measurement systems and the data processing techniques, emphasis has been placed on increasing repeatability of the tests, as well as avoiding user induced errors. The techniques used to achieve this are presented and discussed along with a number of key results and outputs.

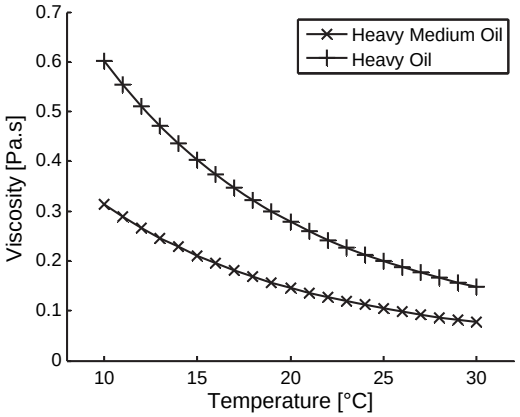

Figure 1. Testing fluid viscosity measurements.

Materials

To demonstrate application of these methodologies in this article, an 800 g/m^2 balanced plain woven (PW) textile has been used. This reinforcement is made from E Glass fibres, with a fibre density of 2.54 g/cm^3 and supplied by Gurit (Asia Pacific) Ltd. Samples comprising 1, 2, 4, 8 and 10 layers are studied at three fibre volume fractions, 0.25, 0.34 and 0.42, with 0.25 being the uncompacted V_f for the textile.

As the resin cure phase of an LCM process is not relevant in the permeability characterisation tests, a Newtonian mineral oil is used as the test fluid in place of a thermoset resin. It is important to ensure that the particular fluid selected will not have particular interactions with the fibrous reinforcements (e.g. water based fluids with natural fibres)[39] and it is generally best practice to measure permeability with a fluid that has properties close to those of the resin to be used. Here, the Mobil DTE series Heavy mineral oil has been used, where its polynomial viscosity model (which is required for the post processing of the permeability data) has been determined using the Parr Physica UDS200 rheometer. For cases where a fluid with lower viscosity is required, a lighter oil (such as the Heavy Medium Oil) can also be used, as shown in Figure 1.

In-plane permeability testing

A 2D in-plane, radial flow permeability test rig has been developed and has been used in a number of previous research works since 2010.[33,40–44]. Radial flow measurements involve compaction of the textile between two platens to the desired V_f and the injection of a fluid via an inlet port located at the centre of the sample. Flow through the reinforcement material follows a radial fluid distribution pattern. Images of the fluid flow front are captured and analysed, computing its velocity, which is then used to determine the

sample's in-plane permeability properties. A radial flow technique is used as the experiments are able to be carried out with relative simplicity. Any problems associated with 'race-tracking' are eliminated and the amount of set-up before each test (as well as cleaning after each test) is minimised. In addition to this, the complete in-plane permeability tensor (K_{11} and K_{22}) along with the angle of orientation are obtained in a single test.

Experimental facility

The 2D in-plane test facility (as shown in Figure 2) is installed on an Instron 1186 universal testing machine

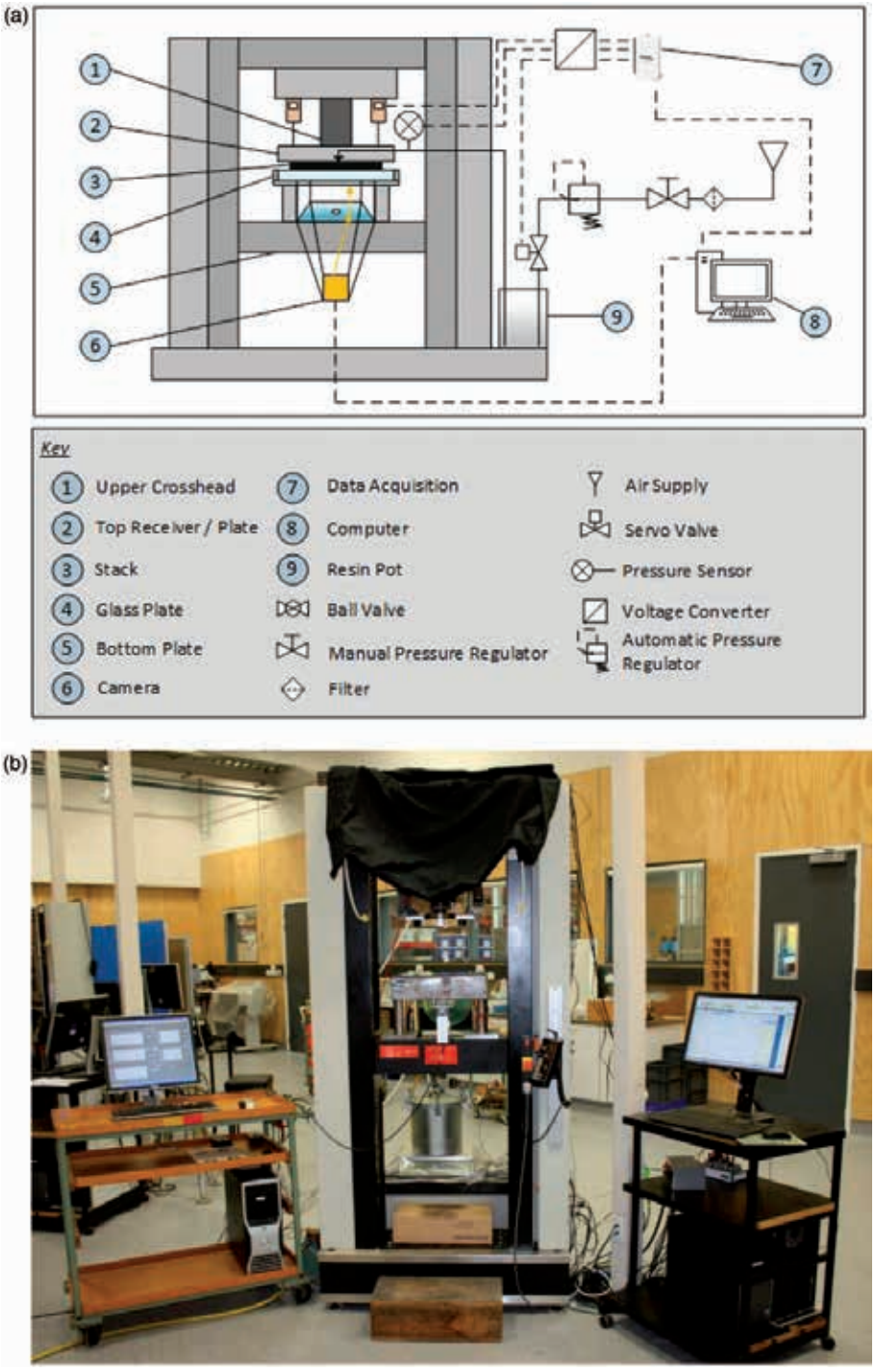

Figure 2. 2D in-plane permeability rig (a) schematic and (b) in the laboratory.

(UTM). A UTM is used as it provides precise control of the platen position (and resulting cavity thickness), as well as a measurement of the total compaction force applied. The compaction data is a significant additional set of information, which provides essential information about the compressibility properties of the textile samples. Obtaining this concurrently to the permeability testing enables the in-depth study of the compaction-permeability relationship.

This highlights the benefit of having the permeability facility installed on a UTM: the compaction response can be obtained concurrently to the permeability testing.

The upper platen is a 250 mm diameter, 30 mm thick aluminium with a 10 mm diameter hole in the centre for fluid injection. The lower platen, constructed out of glass, allows for optical monitoring of the flow front position and is a 350 mm × 55 mm thick square. The clear lower platen allows for optical monitoring of the sample and fluid infiltration throughout the experiments, providing a better understanding of the flow behaviour. Both platens were designed to minimise any deflections during the compaction. A maximum deflection of 0.07 mm is observed under a compaction of 2 MPa. The lower, glass platen has been designed to withstand compaction of up to 2.5 MPa. The platens are shown in Figure 3.

The upper platen is fixed and is aligned relative to the lower platen using a spherical alignment unit (designed based on an MTS Alignment unit model 609.25A) and custom-designed and manufactured strain-gauged compressive alignment specimen developed by Hickey.[45] This achieves parallelism and uniform cavity thickness to a tolerance of 0.005 mm.

Samples are cut into a 270 mm square, with a 15 mm diameter centre hole punched out in order to encourage in-plane flow during the fluid injection. The cutting is performed using a specifically designed square cutting blade in a cutting press. This setup is capable of cutting PW samples of up to 15 layers at once. The specimens are each weighed after being cut using a Sartorius LP12000S digital precision weighing scale prior to the permeability tests.

The position of the lower platen is controlled by the UTM and the cavity thickness achieved monitored by two Mitutoyo 543-515E IDF150 thickness gauges with a resolution of 0.001 mm. Measuring directly between the platens eliminates the effect of compliance in the testing machine and fixture.

The test fluid is injected centrally through the upper platen at a constant pot pressure, regulated using an electronic pressure regulator (Norgren VP50). The fluid gauge pressure is measured at the inlet using a chemical vapour deposition (CVD) pressure transducer (Gems 1200). The manufacturer's stated measurement accuracies for these instruments are listed in Table 1.

Data acquisition. During each of the tests a number of parameters are continuously measured and recorded. The parameters monitored and recorded are:

- Load
- Inlet gauge pressure
- Cavity thickness
- Oil Temperature (inside pot)

A National Instruments USB-6008 DAQ is used to acquire signals from each of the transducers. The load signal is output from the Instron 1186 UTM controller as a ±10 V signal with a full scale that can be tailored to

Table 1. Measurement accuracies.

Measurement	Accuracy
Sample mass	±0.2 g
Mass of oil injected	±0.3 g
Total compaction force	±0.25%
Fluid gauge pressure	±1.00%
Cavity thickness	±0.005 mm

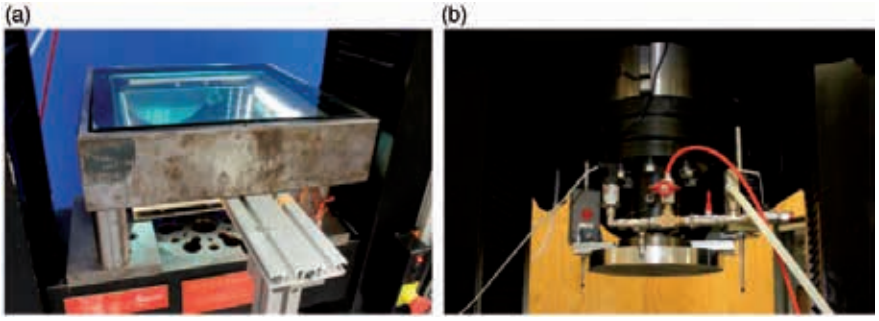

Figure 3. Platens used in the in-plane permeability rig. (a) Lower platen and (b) upper platen.

the specific test run. Here it was set to 30 kN. The Mitutoyo 543-515E IDF150 thickness gauges directly output a ±10 V signal. A custom built signal conditioning unit is used for the CVD pressure transducer, supplying a 0-5 V signal. National Instruments LabVIEW is used to display the output on the monitor in real-time and to write the data captured for post-processing.

Example outputs are shown in Figure 4, where the load, cavity thickness and gauge pressure measurements obtained from conducting in-plane tests on the PW material at different V_f are shown. These values have been normalised to their respective maximum values to enable easy comparison.

As can be observed in Figure 4, there are two components to the measured compaction load: the load associated with textile compaction and the load resulting from injecting the fluid. As expected, the textile compaction load increases with decreasing cavity thickness. The textile is held at the final cavity thickness, the load decreases during this time due to textile relaxation. While the fluid is injected, the load increases again due to the fluid pressure forces. The contribution of each of these components changes with increasing fibre volume fraction. This highlights the benefit of having the permeability facility installed on a UTM: the compaction response can be obtained concurrently to the permeability testing.

Imaging equipment. The flow front progression is monitored using a Navitar SV5C10 digital camera, operating through EPIX PIXCI S14 frame grabber software via a mirror mounted at 45° from the horizontal axis. This set-up is shown in Figure 5(a). Pictures are taken at 1 s intervals for the duration of the test. Each picture has an associated time stamp which is later used for the post processing and correlation to the other acquired data.

The textile sample is lit using four 300 mm 14.4 W/m LED strip lights providing a luminosity of 900 lm/m. These lights are mounted along the internal edges of the lower platen using piano hinges. The angles of the light strips may be adjusted and the light strips can be independently controlled to suit the specific textile tested. Using such a lighting system provides sufficient contrast to detect the flow front, while minimising reflections that would have otherwise been caused from direct light. In addition to this, the LED lights do not generate any significant heat, and hence could be left on continuously during the testing. Raw images of

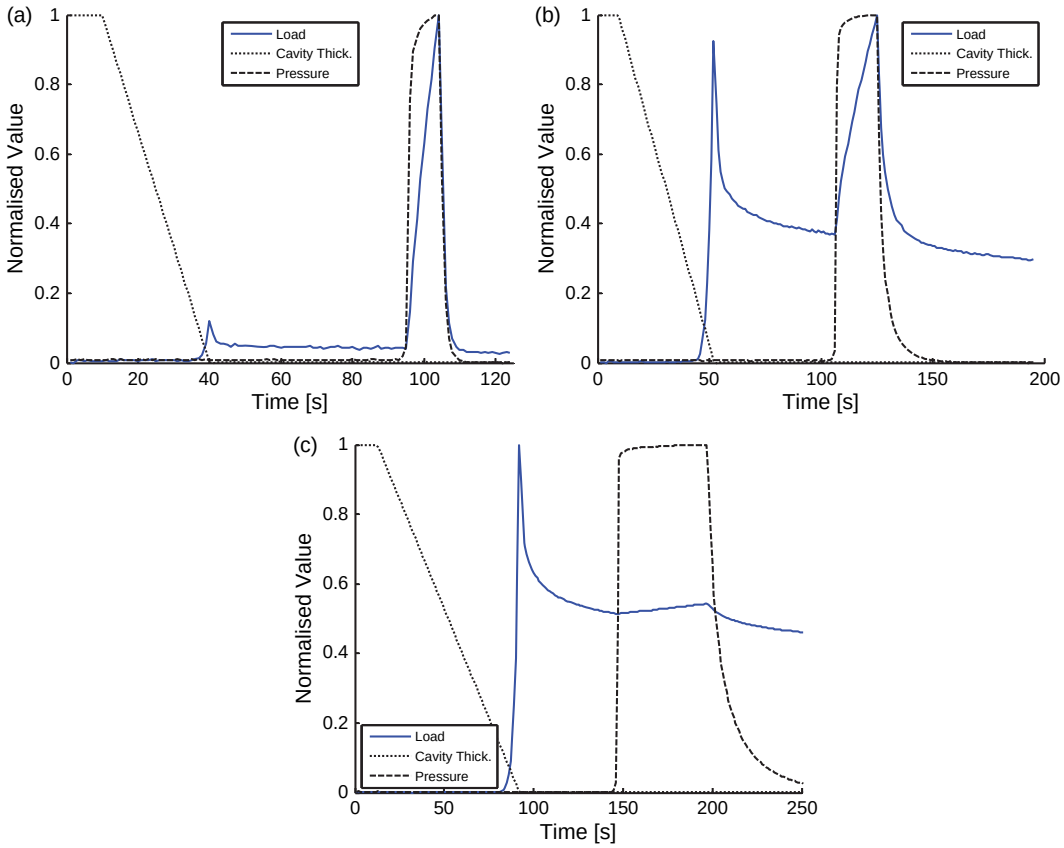

Figure 4. Normalised load, cavity thickness and gauge pressure measurements obtained from PW in-plane tests at (a) 0.25, (b) 0.34 and (c) 0.42 V_f.

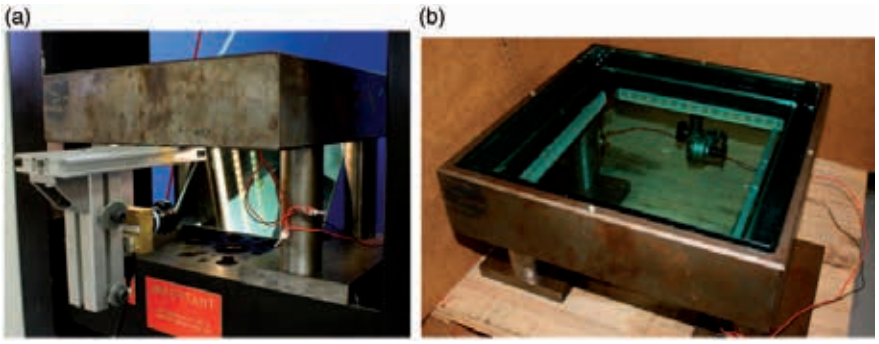

Figure 5. (a) Lower platen with mirror and (b) lighting set.

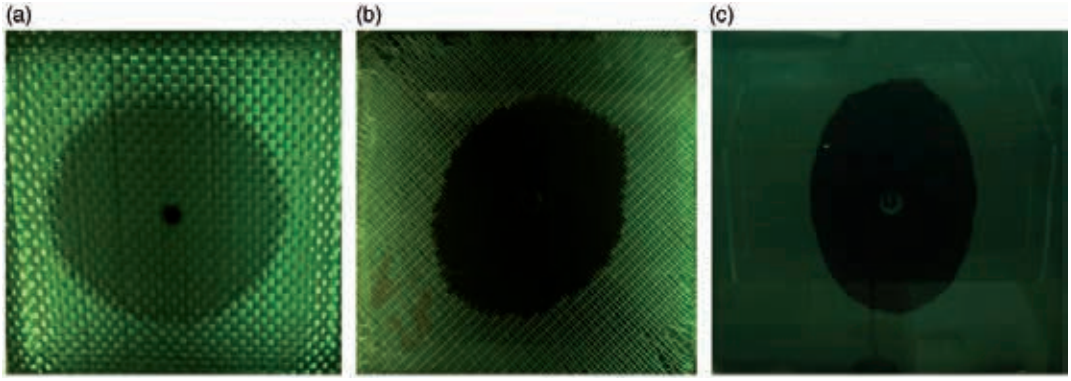

Figure 6. Flow front images of different textiles. (a) Plain woven glass, (b) UD Carbon stitched and (c) UD flax stitched.

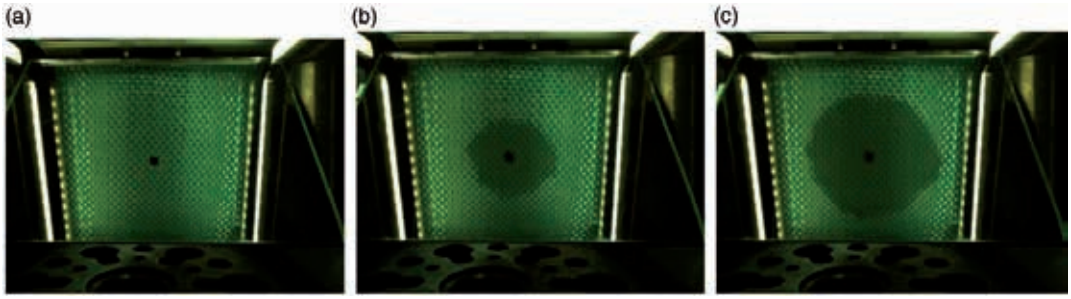

Figure 7. Capturing flow front progression. Eight-layer PW sample compacted to 0.42 V_f at (a) 0, (b) 10 and (c) 30 s after start of injection.

different textiles capture using this lighting system are shown in Figure 6.

The flow front progression can be observed for the testing of an eight-layer PW sample compacted to a V_f of 0.42 in Figure 7. The raw images captured during the testing show the position of the flow front at different time steps.

Data processing

The images obtained are processed to determine the permeability tensor using a set of MATLAB® codes that have been specifically developed. This processing tool enables batch processing (of a large number of samples) and has an associated Graphical User Interface which simplifies use for inexperienced users.

Flow front detection. The flow front of each image is automatically determined through the application of a number of steps which are part of the post-processing tool developed. The raw images are first cropped, rescaled and converted to grey scale to allow for more efficient processing. The images are then calibrated and transformed to correct for distortions caused by the

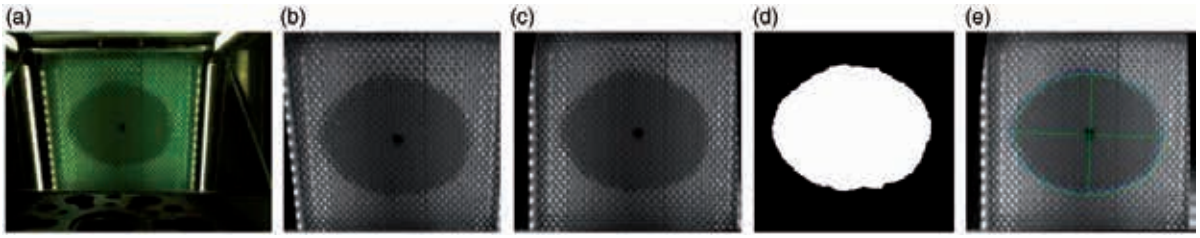

Figure 8. Image processing on flow front images to obtain the permeability tensor. (a) Raw image, (b) image cropped and converted to gray scale, (c) image transformed, correcting for distortion, (d) flow front position identified and (e) ellipse fitted to flow front.

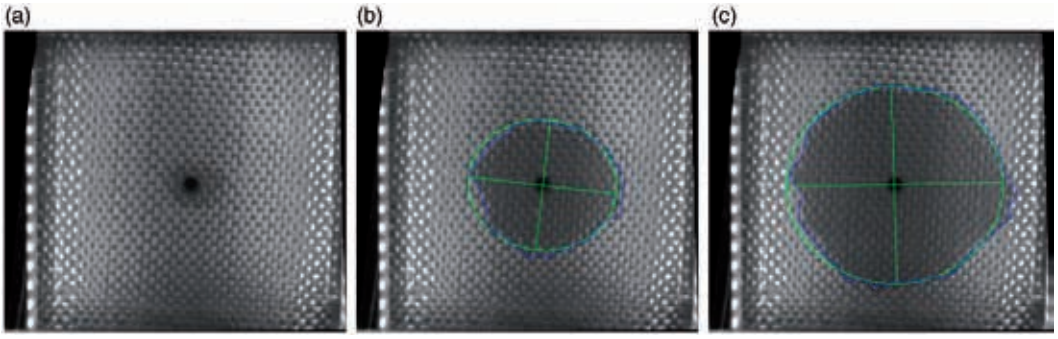

Figure 9. Image processing on flow front images to obtain the permeability tensor. Eight-layer PW sample compacted to 0.42 V_f at (a) 0, (b) 10 and (c) 30 s after start of injection.

mirror angle and lens distortion. The flow front position is then determined by subtracting the current image from the first image. Finally, an ellipse is fitted to the flow front area, using a tool previously developed by Fitzgibbon et al.[46] An example of the progression of these steps is illustrated in Figure 8.

Figure 9 provides examples of analysed image sets of PW samples tested at different V_f (raw images were previously shown in Figure 7). The identified flow front (boundary between the wet and dry areas of the fabric) is shown in blue and the fitted ellipse in green.

Computing permeability. Equations 2 and 3 are the main equations used to compute the in-plane permeability in the principal axis directions. These have been derived by Weitzenbock et al.[47] They were derived from Darcy's law, along with the second order partial differential equation for anisotropy flow pressure distribution (equation (4)).

$$K_{11} = \left\{ a^2 \left[2\ln\left(\frac{a}{r_i}\right) - 1 \right] + r_i^2 \right\} \frac{1}{t} \frac{\mu\varepsilon}{4P} \tag{2}$$

$$K_{22} = \left\{ b^2 \left[2\ln\left(\frac{b}{r_i}\right) - 1 \right] + r_i^2 \right\} \frac{1}{t} \frac{\mu\varepsilon}{4P} \tag{3}$$

$$K_{11} \frac{\partial^2 P}{\partial x^2} + K_{22} \frac{\partial^2 P}{\partial y^2} = 0 \tag{4}$$

In equations (2) and (3), a and b are the flow front ellipse major and minor radii. r_i is the injection inlet radius which in this case is 7.5 mm. μ is the fluid viscosity, determined using the viscosity curves previously obtained along with the measured fluid temperature. ε is the textile sample porosity. This is computed based on the cavity volume and volume of fibre in the sample (determined from the sample's mass and the textile's density). P is the pressure drop which is equal to the injection gauge pressure as the outlet pressure is assumed to be equivalent to atmospheric. t is the time interval from the beginning of injection until the current flow front image analysed.

In the examples presented in this article, the flow front images are recorded at 1s increments while the other data types at a frequency of 100 points per second. The permeability tensor is therefore computed for each flow front image and the data recorded at that time interval. This is illustrated in Figure 10. 20 data points have been computed, using 20 flow front images. Sample permeability is calculated from the average of the last two thirds of the data points. This accounts for any flow stabilisation effects present at the beginning of the test.

Unsaturated in-plane permeability tests

A set of experiments were conducted in order to characterise the in-plane permeability behaviour of single

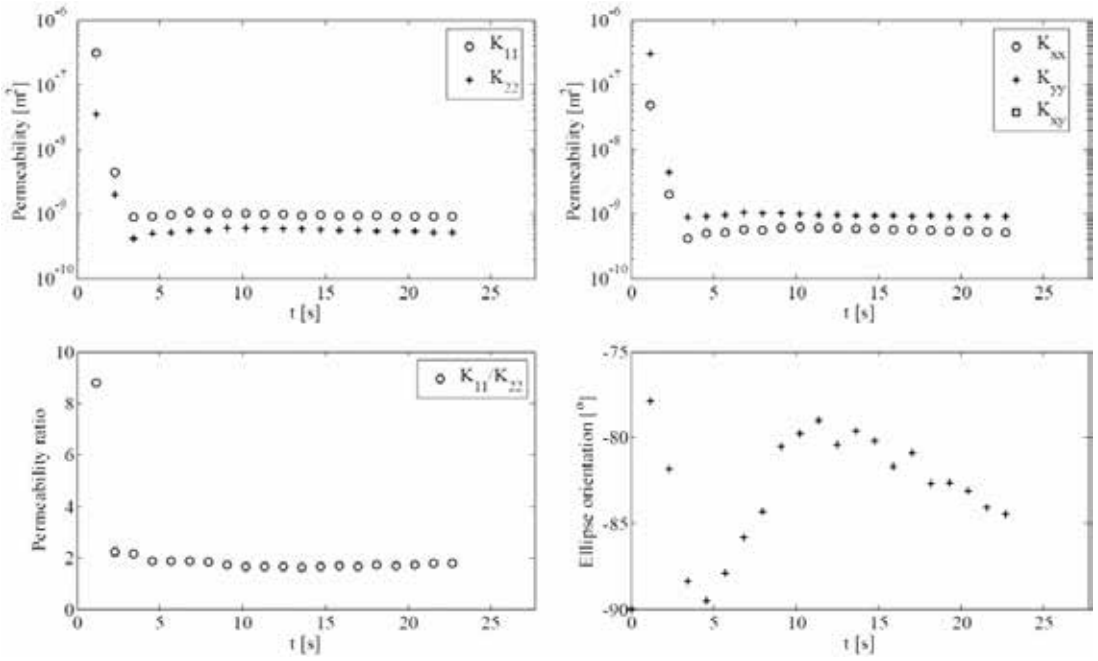

Figure 10. In-plane permeability result output from the analysis of a single sample.

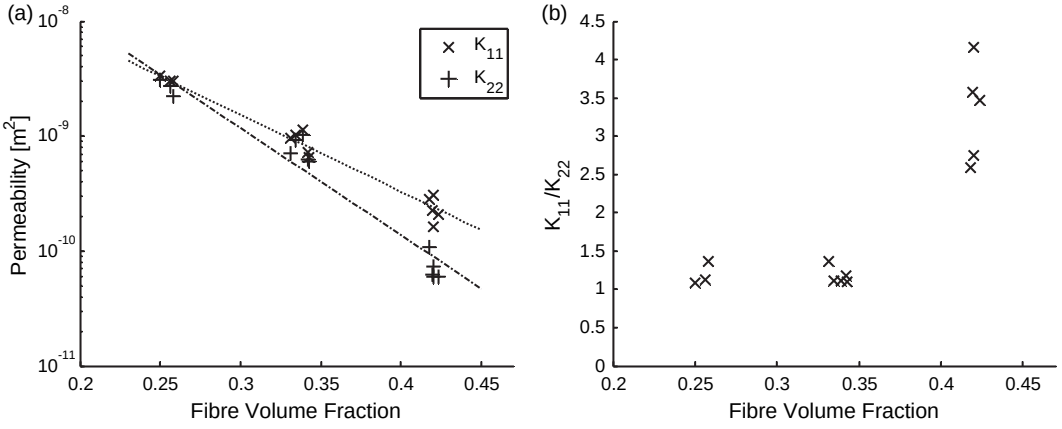

Figure 11. PW permeability characteristics. (a) K_{11} and K_{22} and (b) anisotropy.

and multi-layer PW textile samples. These tests were conducted at three fibre volume fractions: 0.25, 0.34 and 0.42. The first, corresponding to the uncompacted, virgin V_f. Single layer permeability results are plotted against the fibre volume fraction of the samples in Figure 11. Figure 11(a) presents the measured permeabilities in the principle directions of the sample and Figure 11(b) the resulting anisotropy ratio.

An exponential relationship for the principle permeabilities was determined based on equation (5). The resulting parameters, based on a linear regression fit are outlined in Table 2. Coefficients of determination of 0.97 and 0.95 have been achieved for the curve-fitting of K_{11} and K_{22}, respectively, representing a strong correlation. As would be expected, the permeability decreases in both directions with increasing fibre

Table 2. Parameters describing exponential fit to PW permeability data.

Direction	A	B	R^2
K_{11}	1.83E-7	−15.9	0.97
K_{22}	1.10E-6	−22.6	0.95

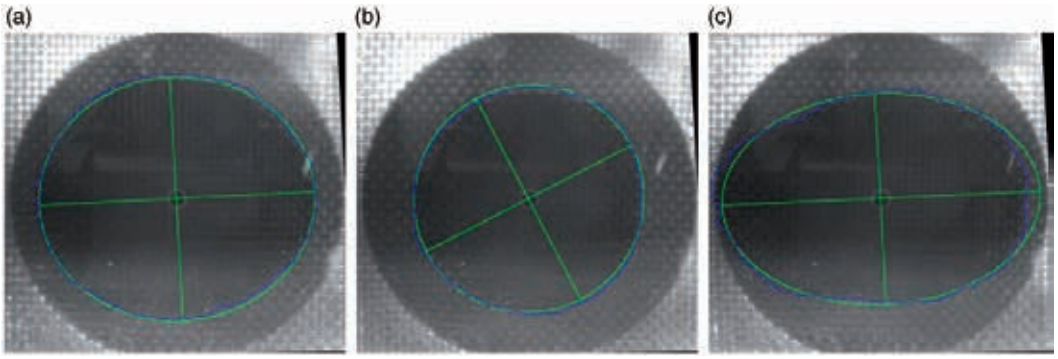

Figure 12. Flow fronts. PW at (a) 0.25, (b) 0.34 and (c) 0.42 V_f.

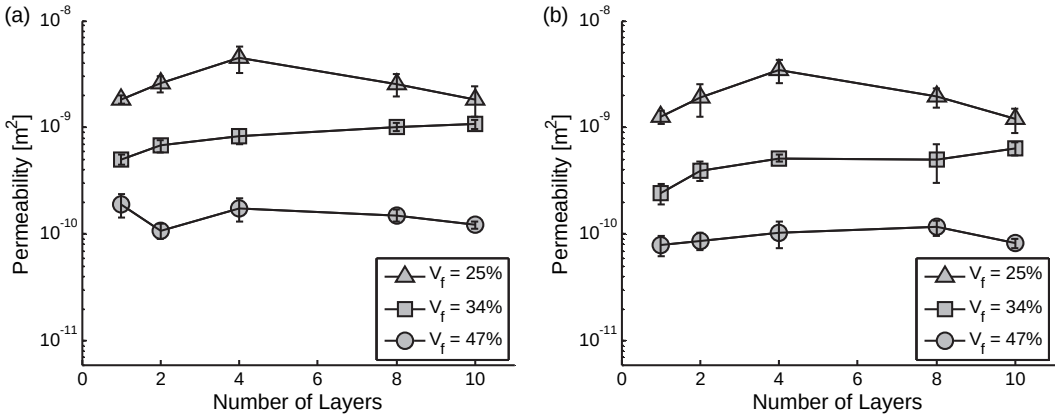

Figure 13. PW multi-layer in-plane tests. (a) K_{11} and (b) K_{22}.

volume fraction. The test data follows the expected exponential-like trend.

$$K = Ae^{BV_f} \tag{5}$$

Figure 11(b) shows the evolution of the anisotropy ratio (K_{11}/K_{22}) with increasing V_f. The anisotropy ratio remains unchanged (at approximately 1.25) at the lower fibre volume fractions tested, however it increases significantly at the higher fibre volume fraction. Figure 12 shows the identified flow fronts for tests at each of the fibre volume fractions. As can be seen, the flow front of the sample at the highest fibre volume fraction is more elliptical as compared with the other two flow fronts.

This is not necessarily a typical behaviour of PW textiles. This may be explained for this particular textile due to the structure of the uncompacted textile. This textile has previously been shown to have a significantly larger tow gap width in the warp than in the weft direction.[48] With increasing compaction, the gap in the weft direction reduces to zero while a gap is still present in the warp direction, contributing to an even more significant difference in the permeabilities in the two directions.

In-plane permeability experiments were also completed on multi-layer samples. A study was undertaken to characterise the permeability of 1, 2, 4, 8 and 10 layer samples at the three fibre volume fractions of interest (0.25, 0.34 and 0.42). Each test was repeated four times to ensure robust results.

The test samples were created by stacking the desired number of layers, in the same orientation. These were then cut at once using the cutting tool and cutting press. No special attention was given to ply-shift, representing realistic conditions within industrial preforms; therefore the final nesting will have some variability. Figure 13(a) and (b) show the average permeability values (along with one standard deviation of the four repeats) obtained in the principle directions, for increasing number of layers at the different fibre volume fractions tested.

Saturated in-plane permeability tests

For cases where the *saturated* permeability data is required, the same set-up may be used to qualitatively study the saturated in-plane flow as well as obtain approximate saturated permeability characteristics.

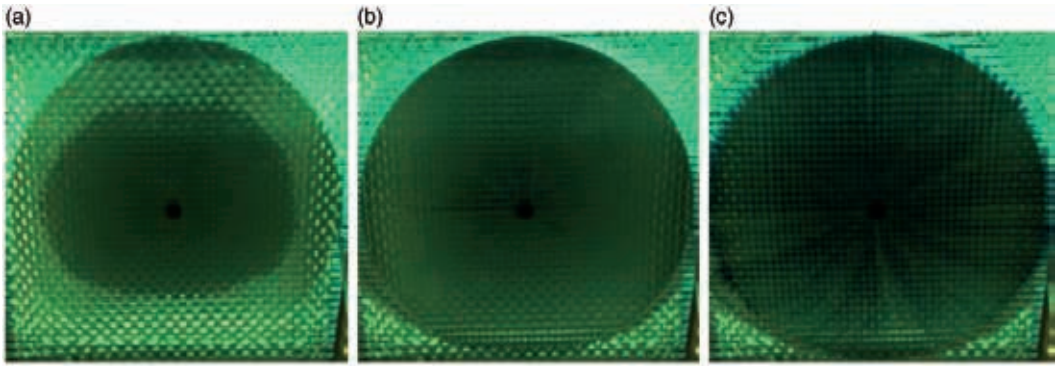

Figure 14. Qualitative in-plane saturated experiments: sequence of raw images captured for the testing of a single layer PW at 0.42 V_f. (a) Unsaturated flow front, (b) saturated sample and (c) saturated flows.

Qualitative tests. Initially a standard unsaturated permeability test is completed on a sample. The sample is brought to full saturation with constant cavity thickness. A coloured testing fluid is then used for further injection. The flow front progression is captured using the same imaging equipment described earlier, and the resulting images enable a better understanding of the saturated flow through the textiles.

For the coloured testing fluid, the same testing fluid is used (Mobil DTE Heavy oil) with the addition of a Glycol based blue tinter (which is normally used to tint household paints). About 10 mL of the tinter was used to colour 4 L of oil to the desired colour level. The viscosity of the oil was not altered upon the addition of the tinter and this was confirmed by measuring it again using the Parr Physica UDS200 rheometer.

Figure 14 shows the unsaturated and saturated flow front propagation for the same sample: a single layer PW textile compacted to a target V_f of 0.42. As can be seen, the tinted oil flows predominantly in the gaps between the tows (as opposed to producing a well-defined ellipse like in the unsaturated tests). This is as expected as the tows are saturated and the fluid flows in the paths of least resistance. The ratio between the flow in the horizontal and vertical directions of the saturated tests appears to be similar to that observed in the unsaturated test, suggesting that the anisotropy ratio remains unchanged irrespective of the level of textile saturation.

Figure 15 provides a clear depiction of the area where the tinted oil flowed during the saturation test injection. This was obtained by subtracting the initial image from the saturated experiment from the current frame and converting to a binary image. Areas in white represent the locations where the tinted oil is present. As can be seen here, the oil has predominantly flowed around the tows rather than through them.

These saturated tests, provide an insight into the saturated flow regime through this textile. They highlight that when fully saturated the flow is predominantly between the fibre tows and not through them (resulting from capillary pressure[49,50]). The irregular shape of the flow front prevents the application of the elliptical flow front technique used for unsaturated flows permeability calculations.

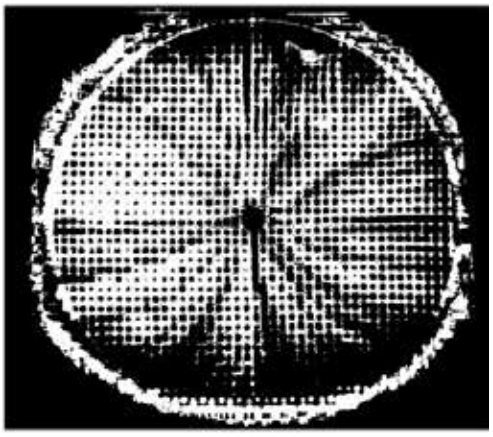

Figure 15. Binary image showing location of tinted oil during the saturated permeability testing of a single layer PW textile compacted to a target V_f of 0.42.

Quantitative tests. These tests are carried out in order to quantify the difference between the samples' unsaturated and saturated permeabilities. Standard in-plane permeability tests are initially conducted, as per the methodology described earlier. Before commencing with the saturated permeability tests, the samples are fully saturated with oil and left for 2 min.

To compute the saturated permeability, additional oil is injected into the sample. The mass of the oil pot is continuously recorded. By fitting a linear regression onto the mass-time curve, the mass flow rate, $\dot{m}$ is determined, and used in equation (6) to compute the saturated permeability of the sample. This equation has

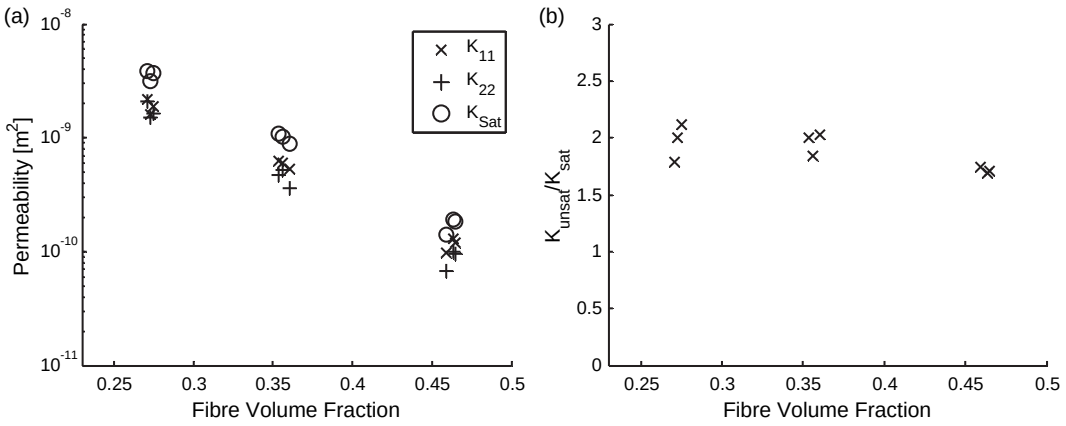

Figure 16. Comparison of saturated and unsaturated permeability behaviour of single layer PW samples.

been derived from Darcy's law. P_{inj} is the injection pressure, μ the fluid viscosity, h the cavity thickness, r_i the internal radius of the sample (of the hole punched in its centre) and r_o the sample's outer radius (taken as the radius of the upper platen).

$$K_{saturated} = \frac{\dot{m}\mu \ln\left(\frac{r_o}{r_i}\right)}{2\pi\rho h P_{inj}} \tag{6}$$

This calculation assumes that the sample is isotropic and the permeability in all directions is equal. This is not the case (as previously shown in Figure 12); however, it still provides a valuable comparison.

Tests were carried out on single layer PW samples at three V_f. Both the saturated and unsaturated permeabilities were calculated for each sample, providing a direct comparison of the two characteristics. Figure 16(a) shows the results obtained. As can be seen, the saturated permeability results are higher than the unsaturated permeability values in the two principle directions.

In order to determine the ratio between the unsaturated and saturated permeabilities of each of the samples, an averaged unsaturated permeability value should first be computed. This was estimated using equation (7), which stems from computing the radius of a circle which has the same area of an ellipse with given principle axes lengths.

$$K = \sqrt{K_{11} \times K_{22}} \tag{7}$$

The resulting ratios are illustrated in Figure 16(b). On average, a ratio of 1.88 was observed. The difference between the unsaturated and saturated permeabilities of textiles can depend on many factors such as the fibre bundle size, spacing and fabric itself. Previous studies have shown that the ratios of saturated to unsaturated permeabilities can range from 0.25 to 4.[51] The ratio computed for the textile studied in the presented work lies within this range.

Through-thickness permeability testing

A 1D through-thickness, saturated flow test rig has been developed and has been used in a number of previous research works since 2012.[33,40,41,45,52] Here, saturated flow permeability measurements are made, enabling several fibre volume fractions to be tested on a single sample. Similar to the in-plane facility, dry reinforcement material is tested using oil as the testing fluid. The through-thickness facility has been designed to also enable the measurement of the through-thickness air permeability of pre-impregnated textiles.

Experimental facility

Figure 17 provides illustrations of the experimental facility that was used to carry out the through-thickness permeability tests. This facility was designed to ensure that maximum rigidity is achieved, thereby eliminating the effects of any deflections during high levels of textile compaction. Circular samples of the textile (130 mm diameter) are placed between two aluminium platens. These platens contain a pattern of 628.2 mm diameter holes creating a through-thickness flow area with a diameter of 100 mm. The hole pattern used creates the most homogeneous flow possible and the permeability of these aluminium platens has been estimated at 1E-8 m^2 (thereby not interfering with the measurement of typical reinforcing textiles). The plates are aligned using a parallelism rig developed by Hickey.[45]

Oil is injected through the thickness direction of the reinforcement material as a result of an applied pressure drop, and the through-thickness permeability is

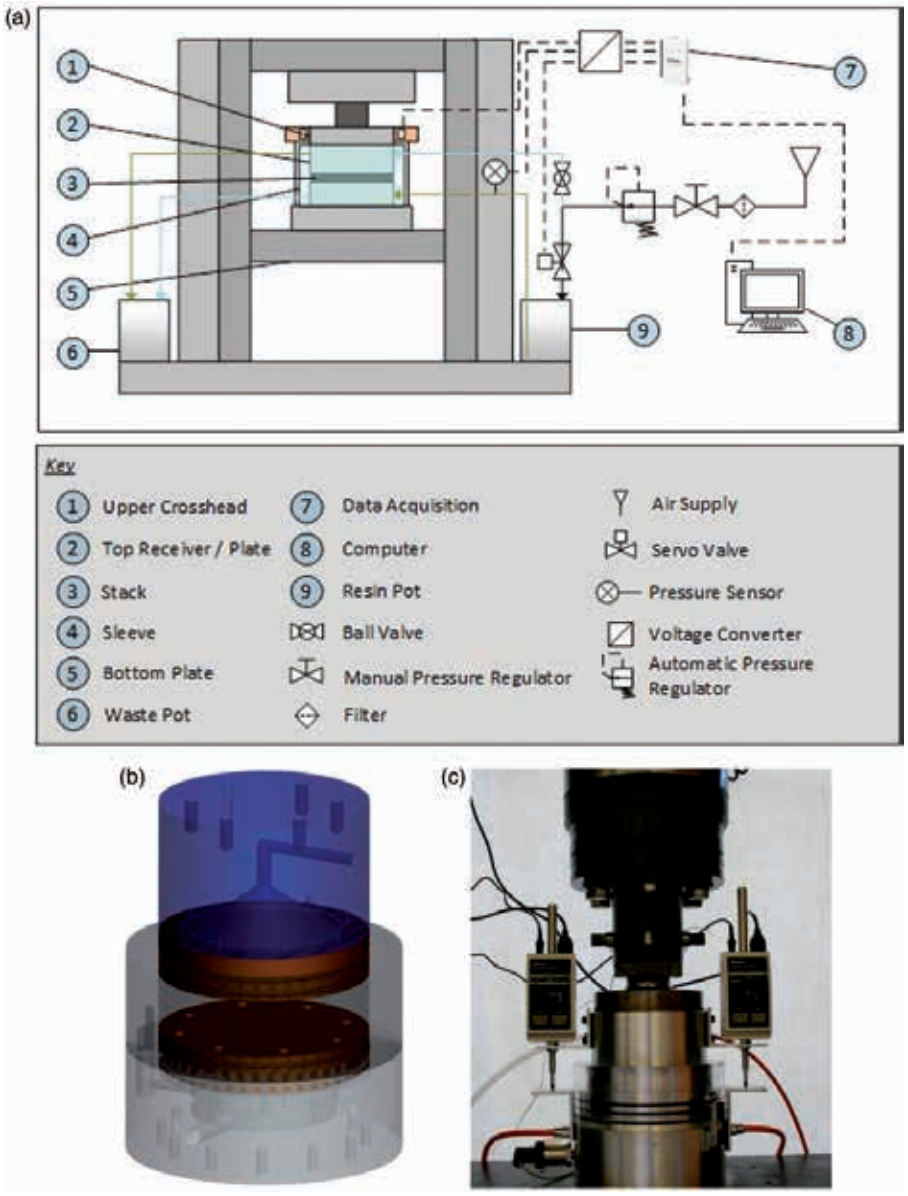

Figure 17. Through-thickness permeability rig (a) schematic, (b) and (c) in the laboratory.

computed from the measured mass flow rate using Darcy's law, as shown in equation (8). The oil flows upwards through the bottom aluminium plate, through the sample and the upper aluminium plate into the upper chamber, and then out to a waste pot.

$$K = \frac{\dot{m}\mu L}{A\rho P} \tag{8}$$

Similar to the in-plane testing facility, the through-thickness permeability test facility is installed on an Instron 1186 UTM. A UTM is used as it provides accurate control of the platen position, as well as a measurement of the total compaction force applied. The achieved cavity thickness is measured by two Mitutoyo thickness gauges with a resolution of 0.001 mm.

The edges of the textile samples tested are sealed by the injection of silicone grease through a series of grease channels. This is done in order to avoid race tracking around the sample. The grease is injected using a manual grease gun until a 0.2 kN increase of force is measured by the load cell. Previous tests have shown that this set up can be used to determine the permeability of samples to an accuracy of 1E-15 m^2.[45]

Two pressure transducers are installed within the device, measuring the pressure in the top and bottom cavities (hence above and below the textile sample). From this, the pressure gradient across the sample can be isolated, ensuring that any pressure losses due to the rig configurations do not affect the results.

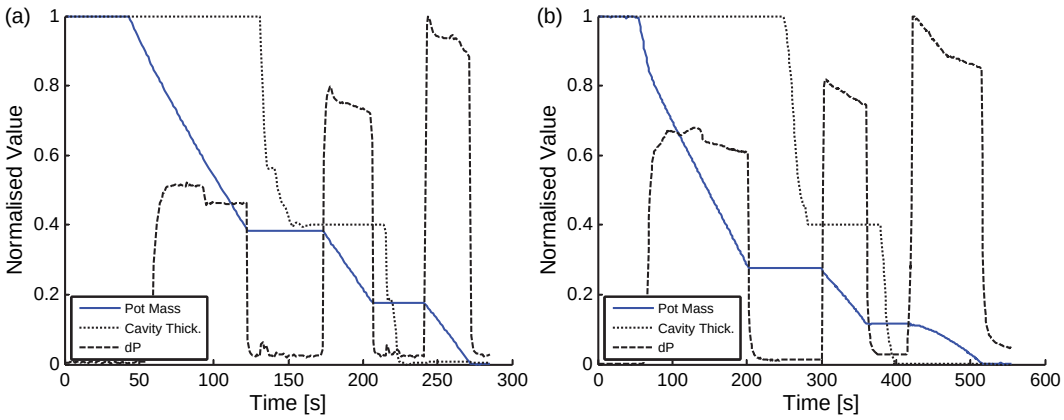

Figure 18. Normalised pot mass, cavity thickness and pressure drop measurements obtained from PW through-thickness tests with (a) two and (b) ten layers.

Data processing

Examples of typical results are displayed in Figure 18 showing the recorded pot mass (the mass of the testing fluid in the pot), cavity thickness and pressure drop measurements for two tests.

These files are processed to compute the resulting permeability using equation (8). As each test was conducted on the three fibre volume fractions, it is important to select the correct range of data for each measurement. This is carried out through a graphical user interface, where the user selects the range. This normally falls in the region where the pressure drop has settled during the fluid injection. This analysis is carried out using MATLAB® codes, enabling batch processing of a large number of samples. The scripts are incorporated in a graphical user interface enabling inexperienced users to use it efficiently.

Experimental results

Through-thickness permeability testing was carried out on PW samples with varying number of layers at three fibre volume fractions. Figure 19 shows the average permeability results obtained. As expected, the through-thickness permeability decreases with increasing V_f. Interestingly, the permeability also decreases with increasing number of layers. This may occur due to the increased level of nesting present in preforms with greater number of layers: the likelihood of the flow channels being blocked increases, thus decreasing the permeability.

These tests were conducted using an injection pressure of 150 kPa. Although this injection flow could have resulted in hydrodynamic compaction (thereby increasing the samples' V_f and affecting the permeability),[53,54] analysis of the measured compaction pressures applied to the samples showed that these were consistently higher than the injection pressure. This provides further confidence that the samples were continuously compacted by the perforated aluminium plates, eliminating the effects of hydrodynamic compaction.

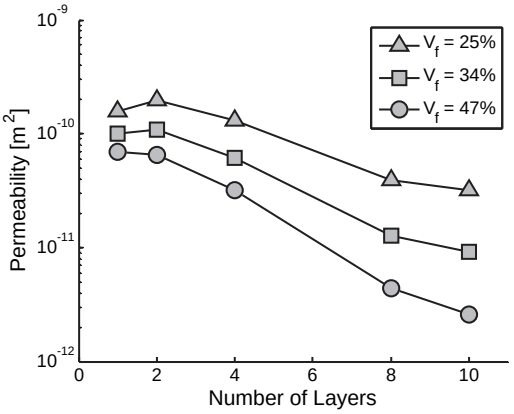

Figure 19. PW multi-layer through-thickness permeability test results.

Conclusions

Two measurement systems used to characterise the permeability of fibre reinforced textiles in an efficient and robust method have been presented. Both measurement systems are installed on a UTM, providing continuous control and measurement of the applied compaction, enabling the testing of any cavity thickness and resulting V_f. A spherical alignment unit is also used, ensuring parallelism and uniform cavity thickness to 0.005 mm.

In-plane permeability tests are carried out on unsaturated samples, using a radial flow injection scheme. Radial flow enables the determination of the full 2D permeability tensor from a single test, contributing to the testing methodology efficiency. In addition to this, the tests are much simpler and quicker to carry out to

traditional 1D flow experiments as any problems associated with race tracking are avoided and the cleaning processes between tests is fast and efficient. The flow front is captured visually through the clear lower platen, providing a comprehensive understanding of the flow behaviour.

The flow front images and peripheral data captured from the tests is processed to determine the permeability tensor. This is carried out using a set of MATLAB® codes that have been specifically developed for the purpose. The processing tool enables batch processing of a large number of samples, and has an associated graphical user interface to aid inexperienced users.

The in-plane permeability rig can also be used to gain an understanding of the textiles' saturated permeability. Techniques used to determine the saturated permeability behaviour both qualitatively and quantitatively have been presented. This provides a simple estimation of the unsaturated-saturated ratio of the textiles and enables the visualisation of the saturated flow path. The qualitative analysis highlighted that, during the saturated flow, the fluid flows predominantly through the gaps between the tows (rather than within the tows). The quantitative tests conducted estimated the unsaturated-saturated permeability ratio for the PW textile at 1.88.

A 1D, saturated flow rig has been developed for the through-thickness testing of textiles. Saturated flow permeability measurements are made, enabling several fibre volume fractions to be tested for a single sample. The oil is injected in the thickness direction of the reinforcement material through a pair of perforated aluminium plates and a unique sealing mechanism is used to avoid race tracking. Test measurements are automatically recorded and this data is processed using MATLAB® codes. Batch processing of a large number of samples is possible, ensuring that the processing is carried out efficiently.

Both the in-plane and through-thickness rigs presented in this work, have been developed over a number of years to ensure that the most efficient testing procedure is achieved. This article provides detail about the experimental devices as well as the post processing techniques used, ensuring that repeatable and robust permeability data is obtained, while ensuring that the processes are simple and quick to carry out and any user-induced errors are minimised. By using the experimental techniques presented, a greater understanding into the permeability behaviour of textiles can be obtained, which can then be used in LCM process simulations to ensure that high quality FRPC parts are manufactured under optimal conditions.

Declaration of conflicting interests

The author(s) declared no potential conflicts of interest with respect to the research, authorship, and/or publication of this article.

Funding

The author(s) received no financial support for the research, authorship, and/or publication of this article.

References

1. Trochu F, Ruiz E, Achim V, et al. Advanced numerical simulation of liquid composite molding for process analysis and optimization. *Compos Part A Appl Sci Manuf* 2006; 37: 890–902.
2. Trochu F, Gauvin R and Gao DM. Numerical analysis of the resin transfer molding process by the finite element method. *Adv Polym Technol* 1993; 12: 329–342.
3. Darcy H. *Les Fontaines Publiques de la Ville de Dijon*. Dalmont, Paris: Victor Dalmont, 1856.
4. Govignon Q, Bickerton S and Kelly PA. Simulation of the reinforcement compaction and resin flow during the complete resin infusion process. *Compos Part A Appl Sci Manuf* 2010; 41: 45–57.
5. Rebenfeld L. Permeability characteristics of multilayer fiber reinforcements. Part I: experimental observations. *Polym Compos* 1991; 12: 179–185.
6. Binétruy C, Hilaire B and Pabiot J. The interactions between flows occurring inside and outside fabric tows during RTM. *Compos Sci Technol* 1997; 57: 587–596.
7. Sharma S and Siginer DA. Permeability measurement methods in porous media of fiber reinforced composites. *Appl Mech Rev* 2010; 63: 1–19.
8. Ahn SH, Lee WI and Springer GS. Measurement of the three-dimensional permeability of fiber preforms using embedded fiber optic sensors. *J Compos Mater* 1995; 29: 714–733.
9. Bréard J, Saouab A and Bouquet G. Dependence of the reinforcement anisotropy on a three dimensional resin flow observed by X-ray radioscopy. *J Reinf Plast Compos* 1999; 18: 814–826.
10. Buntain M and Bickerton S. Compression flow permeability measurement: a continuous technique. *Compos Part A Appl Sci Manuf* 2003; 34: 445–457.
11. Elbouazzaoui O, Drapier S and Henrat P. An experimental assessment of the saturated transverse permeability of non-crimped new concept (NC2) multiaxial fabrics. *J Compos Mater* 2005; 39: 1169–1193.
12. Endruweit A, Luthy T and Ermanni P. Investigation of the influence of textile compression on the out-of-plane permeability of a bidirectional glass fiber fabric. *Polym Compos* 2002; 23: 538.
13. Ferland P, Guittard D and Trochu F. Concurrent methods for permeability measurement in resin transfer molding. *Polym Compos* 1996; 17: 149–158.
14. Gantois R, Jourdain E and Dusserre G. Recent patents on in-plane permeability measurement of lcm composite reinforcements. *Recent Pat Eng* 2009; 3: 109–116.
15. Hoes K, Dinescu D, Sol H, et al. New set-up for measurement of permeability properties of fibrous reinforcements for RTM. *Compos Part A Appl Sci Manuf* 2002; 33: 959–969.

16. Kuentzer N, Simacek P, Advani SG, et al. Permeability characterization of dual scale fibrous porous media. *Compos Part A Appl Sci Manuf* 2006; 37: 2057–2068.
17. Liu Q, Parnas RS and Giffard HS. New set-up for in-plane permeability measurement. *Compos Part A Appl Sci Manuf* 2007; 38: 954–962.
18. Lundström T, Toll S and Håkanson J. Measurement of the permeability tensor of compressed fibre beds. *Transport Porous Med* 2002; 47: 363–380.
19. Luo Y, Verpoest I, Hoes K, et al. Permeability measurement of textile reinforcements with several test fluids. *Compos Part A Appl Sci Manuf* 2001; 32: 1497–1504.
20. Mekic S, Akhatov I and Ulven C. A radial infusion model for transverse permeability measurements of fiber reinforcement in composite materials. *Polym Compos* 2009; 30: 907–917.
21. Nedanov PB and Advani SG. A method to determine 3D permeability of fibrous reinforcements. *J Compos Mater* 2002; 36: 241–254.
22. Ouagne P and Bréard J. Continuous transverse permeability of fibrous media. *Compos Part A Appl Sci Manuf* 2010; 41: 22–28.
23. Scholz S, Gillespie JW and Heider D. Measurement of transverse permeability using gaseous and liquid flow. *Compos Part A Appl Sci Manuf* 2007; 38: 2034–2040.
24. Wu X, Li J and Shenoi R. A new method to determine fiber transverse permeability. *J Compos Mater* 2007; 41: 747–756.
25. Weitzenböck JR, Shenoi RA and Wilson PA. Measurement of principal permeability with the channel flow experiment. *Polym Compos* 1999; 20: 321–335.
26. Gauvin R, Kerachni A and Fisa B. Variation of mat surface density and its effect on permeability evaluation for RTM modelling. *J Reinf Plastics Compos* 1994; 13: 371–383.
27. Chan AW, Larive DE and Morgan RJ. Anisotropic permeability of fiber preforms: constant flow rate measurement. *J Compos Mater* 1993; 27: 996–1008.
28. Heardman E, Lekakou C and Bader M. Flow monitoring and permeability measurement under constant and transient flow conditions. *Compos Sci Technol* 2004; 64: 1239–1249.
29. Kim SK and Daniel IM. Determination of three-dimensional permeability of fiber preforms by the inverse parameter estimation technique. *Compos Part A Appl Sci Manuf* 2003; 34: 421–429.
30. Gauvin R and Chibani M. The modelling of mold filling in resin transfer molding. *Int Polym Process* 1986; 1: 42–46.
31. Um M and Lee W. A study on permeability of unidirectional fiber beds. *J Reinf Plast Compos* 1997; 16: 1575–1590.
32. Bickerton S and Abdullah MZ. Modeling and evaluation of the filling stage of injection/compression moulding. *Compos Sci Technol* 2003; 63: 1359–1375.
33. Liotier PJ, Govignon Q, Swery E, et al. Characterisation of woven flax fibres reinforcements: effect of the shear on the in-plane permeability. *J Compos Mater* 2015; 49(27): 3415–3430.
34. Gebart BR and Lidström P. Measurement of in-plane permeability of anisotropic fiber reinforcements. *Polym Compos* 1996; 17: 43–51.
35. Lee Y, Wu J, Hsu Y, et al. A prediction method on in-plane permeability of mat/roving fibers laminates in vacuum assisted resin transfer molding. *Polym Compos* 2006; 27: 665–670.
36. Cai Z. Analysis of mold filling in RTM process. *J Compos Mater* 1992; 26: 1310–1338.
37. Vernet N, Ruiz E, Advani SG, et al. Experimental determination of the permeability of engineering textiles: Benchmark II. *Compos Part A Appl Sci Manuf* 2014; 61: 172–184.
38. Arbter R, Beraud JM, Binétruy C, et al. Experimental determination of the permeability of textiles: a benchmark exercise. *Compos Part A Appl Sci Manuf* 2011; 42: 1157–1168.
39. Umer R, Bickerton S and Fernyhough A. Modelling the application of wood fibre reinforcements within liquid composite moulding processes. *Compos Part A Appl Sci Manuf* 2008; 39: 624–639.
40. Liotier PJ, Govignon Q, Swery EE, et al. Permeability of sheared woven flax fibres reinforcements: permeability measurements of the orthotropic behaviour. In: *FPCM 12: 12th International conference on flow processes in composite materials*, Twente, The Netherlands, 2014.
41. Liotier PJ, Govignon Q, Swery EE, et al. Permeability of sheared woven flax fibres reinforcements: definition of parameters to model complex shape composites part processing by LCM. In: *ECCM 16: European Conference on Composite Materials*, Seville, Spain, 2014.
42. Comas-Cardona S, Cosson B, Bickerton S, et al. An optically-based inverse method to measure in-plane permeability fields of fibrous reinforcements. *Compos Part A Appl Sci Manuf* 2014; 57: 41–48.
43. Tournier L. *Method for optical measure of local reinforcement permeability and infusion behaviour prediction in liquid molding processes*. Centre for Advanced Composite Materials, The University of Auckland, 2010.
44. Zhang F, Comas-Cardona S and Binétruy C. Statistical modeling of in-plane permeability of non-woven random fibrous reinforcement. *Compos Sci Technol* 2012; 72: 1368–1379.
45. Hickey CMD. The Influence of Variation in Process Parameters on the Manufacturing of Advanced Fibre Composites, PhD, Mechanical Engineering, The University of Auckland, Auckland, 2014.
46. Fitzgibbon A, Pilu M and Fisher RB. Direct least square fitting of ellipses. *IEEE Trans Pattern Anal Mach Intell* 1999; 21: 476–480.
47. Weitzenböck JR, Shenoi RA and Wilson PA. Radial flow permeability measurement Part A: theory. *Compos Part A Appl Sci Manuf* 1999; 30: 781–796.
48. Swery EE, Allen T and Kelly PA. Automated tool to determine geometric measurements of woven textiles using digital image analysis techniques. *Text Res J* 2015. Epub ahead of print 15 July 2015, doi: 10.1177/0040517515595031.
49. Verrey J, Michaud V and Månson JAE. Dynamic capillary effects in liquid composite moulding with non-crimp fabrics. *Compos Part A Appl Sci Manuf* 2006; 37: 92–102.
50. Pucci MF, Liotier PJ and Drapier S. Capillary wicking in a fibrous reinforcement – orthotropic issues to determine

the capillary pressure components. *Compos Part A Appl Sci Manuf* 2015; 77: 133–141.
51. Bréard J, Henzel Y, Trochu F, et al. Analysis of dynamic flows through porous media. Part I: comparison between saturated and unsaturated flows in fibrous reinforcements. *Polym Compos* 2003; 24: 391–408.
52. Cohades A. *LCM (liquid composite moulding) processing of nanofibre enhanced textile reinforcements*. Switzerland: Masters of Engineering, Laboratoire de Technologie des Composite et Polymers, Ecole Polytechnique Federale de Lausanne, 2012.
53. Becker D, Broser J and Mitschang P. An experimental study of the influence of process parameters on the textile reaction to transverse impregnation. *Polym Compos* Epub ahead of print 28 March 2015, doi: 10.1002/pc.23479.
54. Becker D and Mitschang P. Influence of preforming technology on the out-of-plane impregnation behavior of textiles. *Compos Part A: Appl Sci Manuf* 2015; 77: 248–256.